Probabilistic seismic performance and loss evaluation of a multi-story steel building equipped with butterfly-shaped fuses

Preprint · May 2020

CITATIONS
0

READS
139

2 authors:

Mohsen Zaker Esteghamati
Virginia Polytechnic Institute and State University
9 PUBLICATIONS **13** CITATIONS

SEE PROFILE

Alireza Farzampour
Virginia Polytechnic Institute and State University
34 PUBLICATIONS **171** CITATIONS

SEE PROFILE

Probabilistic seismic performance and loss evaluation of a multi-story steel building equipped with butterfly-shaped fuses

Mohsen Zaker Esteghamati[1] and Alireza Farzampour[2]

[1] PhD Candidate, Department of Civil and Environmental Engineering, Virginia Polytechnic Institute, and State University, Blacksburg, Virginia
[2] PhD, Department of Civil and Environmental Engineering, Virginia Polytechnic Institute, and State University, Blacksburg, Virginia

Abstract. Shear fuses are structural elements that protect surrounding members from damages by undergoing substantial yielding, and then are easily replaced after a major earthquake event. A promising type of structural fuses is butterfly-shaped shear fuse, which can effectively align member's flexural capacity to the imposed moment demand due to its unique geometry. Although recent studies suggest that butterfly-shaped fuses exhibit substantial ductility and energy dissipation, their impact on the global performance of multi-story buildings requires further investigation. This study presents a comprehensive risk-based evaluation of a six-story eccentrically braced steel frame retrofitted with butterfly-shaped fuses. Two nonlinear finite element models of the original prototype building and retrofitted building with butterfly-shaped fuses are developed in OpenSees and incremental dynamic analysis is conducted. The results are used to derive global and story-based fragility and seismic demand hazard curves. Furthermore, earthquake-induced losses associated with structural and non-structural assemblies are quantified and the impact of butterfly-shaped fuses on the distribution of story acceleration and drift demands are evaluated.
The results show that butterfly-shaped fuses significantly improve the structure's performance in terms of all drift-related damage states and the improvement is more pronounced at severe damage states. On the other hand, although the butterfly-shaped fuses reduce the peak floor acceleration at slight damage state, their impact is negligible at higher damage states. In particular, the risk of exceeding complete damage state in the building's lifetime is reduced to approximately one-fourth of the original building's values. Furthermore, shear fuses effectively mitigate weak story formation at lower stories due to their large energy dissipation and ductility. Subsequently, the improved drift-related performance reduces the drift-induced loss of structural and non-structural assemblies, resulting in 44.64% smaller total annual loss for the retrofitted building.

Keywords: Performance-based earthquake engineering · Butterfly-shaped shear fuses · Fragility assessment · Seismic retrofitting · Incremental dynamic analysis

1 Introduction

In the last decade, greater exposure to natural hazards due to population growth and fast-changing environment led to direct and indirect losses and communities' vulnerability; which is projected to be increased substantially by the end of the century [1,2]. Therefore, a wide attention is given to improve infrastructures' resiliency against natural hazards to ensure their ability to withstand extreme conditions while rapidly recovering to the original state [3,4]. An efficient approach for seismic resiliency is to implement novel protective structural systems that enhance buildings' energy dissipation, minimize structural and non-structural damages, and reduce the recovery period [5]. Recent innovative systems such as crescent-shaped brace (a hysteretic bracing system capable of

achieving several performance objectives simultaneously) [6,7] and strongback (a vertical truss connected to the main frame to eliminate weak story formation) [8,9,10] are examples of such initiative, and demonstrate structural engineering's momentum to capitalize on structural forms for achieving enhanced performance under natural hazards.

Among different methods to improve seismic resiliency (e.g.[11,12,13,14,15,16,17,18] to name a few), shear fuses provide a viable solution [19,20]. Shear fuses protect surrounding structural components through yielding, and then are easily replaced after a major earthquake, which minimizes the disruption to the buildings' post-earthquake functionality [21,22]. As a result, different types of structural fuses are incorporated in various seismic-resistant applications for localizing the yielding mechanism and preventing the brittle limit states[23]; preventing high inelastic concentration at the connection area under large drifts; promoting flexural yielding limit state as the major limit state in the web of the beams[24,25]; protecting surrounding members from damages and plastic strains [26]; and increasing the energy dissipation in self-centering systems [27].

A promising form of structural fuses recently described in literature consists of a steel plate with diamond-shaped cutouts leaving butterfly-shaped fuses that could align bending strength with the applied moment. Figure 1 shows a typical butterfly-shaped fuse. The tapered shape of links leads to flexural yielding under shear force, where the flexural strength changes quadratically along the link length. Therefore, the geometry of links can be adjusted to achieve yielding at a more favorable place, such as far from sharp edges, to eliminate the concentration of nonlinearity and improve fracture resistance[28]. In addition, modifying links geometry in terms of taper's slope (L/2a in Figure 1.b) leads to a well-distributed yielding mechanism throughout links, which subsequently increase ductility and energy dissipation[28]. In particular, structures with butterfly-shaped fuses have shown to dissipate energy up to five times larger than the conventional systems for a specific story under the seismic loads[27], making them a desirable structural system for use in seismic rehabilitation and retrofitting of multi-story frames as shown in Figure 2.

Despite the large body of literature addressing structural fuses, only a few experimental and numerical studies investigated the structural performance of butterfly-shaped fuses. Ma et al. performed an experimental study on a series of specimens containing five steel plates with straight cutouts (referred to as "slit fuses") and butterfly-shaped fuses with different geometric configurations. It is shown that the butterfly-shaped fuses have larger deformation capacity and reach higher strength at the tension mode, whereas both types of fuses demonstrate excellent hysteretic behavior for shear demands less than 3% [27]. Through previous computational investigations on steel plates with different cutout shapes, it is shown that the plate with butterfly-shaped cutouts had two times larger ductility and energy dissipation than the plate with bar-shaped cutouts (i.e. strip fuses)[29].

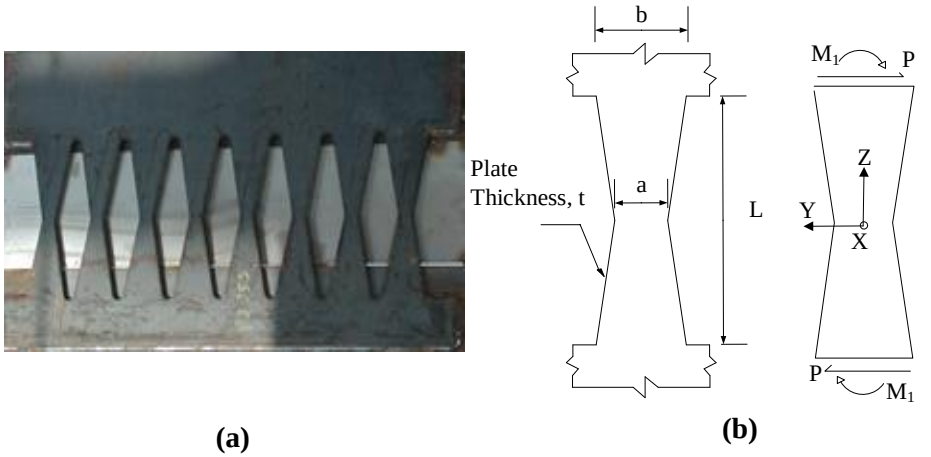

Fig. 1: Butterfly-shaped fuses: (a) fabricated specimen (b) schematic geometry and applied loading

Fig. 2: Several structural applications of butterfly-shaped fuses[30]

Along the same lines, Oh et al. implemented slit fuses at the beam-to-column connection and concluded that the plastic deformation was mainly concentrated at the fuses[31], keeping the plastic deformation far from the connections. Among a few numerical studies, Bayat and Shekastehband investigated connections strengthened using butterfly-shaped and prismatic slit shear fuses and concluded that the strengthened connections show up to 63%, 94%, and 35% higher strength, stiffness,and energy dissipation, respectively[32]. Farzampour and Eatherton studied the effect of butterfly geometry on the load-resisting behavior of the fuses and concluded that taper ratios significantly impact yielding location and inelastic deformation capacity[33]. It is previously determined that butterfly-shaped fuses could withstand cyclic loading up to the 30% shear angle due to the uniform distribution of the stresses across the length of links, limiting the potential of fracture and rapid strength degradation[34].

While previous studies highlighted the advantages of butterfly-shaped fuses from a component-level perspective, further research is needed to quantify the global performance of multi-story structures retrofitted with these fuses. Performance-based earthquake engineering (PBEE) is a conditional probabilistic framework that uses quantitative measures to evaluate structural performance under seismic loads[35,36,37,38]. To this end, time-history analysis is performed on analytical models of structures, and seismic fragility is obtained to represent the conditional probability distribution of exceeding a global damage level at different levels of ground motion shaking intensity. This performance metric can then be directly used to compare different systems, integrated over the site's hazard distribution to obtain annualized seismic risk, or implemented to derive economic or human

vulnerability (i.e. loss) metrics for decision-making applications[39]. Therefore, PBEE-based assessment facilitates a wider representation of structural performance to a larger group of stakeholders, and is the first step towards resilience-based community assessment and planning.

This study aims to evaluate the effect of butterfly-shaped shear fuses on the seismic performance of multi-story steel braced buildings using the PBEE framework. Different performance measures, ranging from structures' demand parameters to economic loss, are adopted to establish a comprehensive comparison, and to identify the extent of butterfly-shaped fuses' impacts. After establishing nonlinear finite element models for steel braced and butterfly-shaped fuses retrofitted systems, incremental dynamic analysis is conducted, and fragility curves are derived for four different performance levels. The obtained fragility curves are combined with the site's hazard to obtain the annual risk of exceeding different limit states. Subsequently, story-based fragilities are derived to evaluate the impact of butterfly-shaped fuses on the story mechanism. Lastly, loss assessment is performed to investigate the economic feasibility of butterfly-shaped fuses. The results of this study are expected to demonstrate butterfly-shaped shear fuses capabilities to retrofit multi-story steel buildings, and to fill the current knowledge gap between local behavior of butterfly-shaped shear fuses and the seismic performance of mid-rise steel structures retrofitted with these devices.

2 Numerical modeling

2.1 Prototype building description

A prototype 6-story steel eccentrically braced frame (EBF) is adopted from the SEAOC example manual[40] to study the behavior of multi-story buildings retrofitted with butterfly-shaped fuses. Figure 3.a shows the schematic configuration of the selected EBF frame. The considered building is assumed to be located in Los Angeles, California, at a site class D with shear wave velocity of 259 m/s which corresponds to the high seismic design category (D_{max}). The prototype building has a six-story eccentrically braced system at each direction and the typical story height is 3.67 m. Details of the conventional EBF seismic design and structural detailing of the prototype building are previously established[40].

As shown in Figure 3.b, the original building is subsequently upgraded by replacing the linking beams of EBF with butterfly-shaped fuses at each story. For this purpose, story shear forces of EBF building are extracted from the SEAOC example manual and used to design the butterfly-shaped fuses following the methodology described in [34]. In this approach, the lateral-torsional buckling is prevented and butterfly-shaped fuses are designed based on flexural yielding at the quarter-point across the length of the link [34]. As shown in Figure 3, different butterfly-shaped fuses are developed for lower stories (Group I for story1 to 3), middle story (Group II for story 4) and upper stories (Group III for story 5 and 6), where the plates' thicknesses are 2.2 cm, 1.7 cm, and 1.2 cm, respectively. Each fuse consists of 10 shear links and the spacing between cutouts is kept at 12 cm and 4 cm at the middle. The width of the links at the ends and the middle is 12 cm and 3.8 cm, respectively, whereas the length of links is 30 cm.

2.2 Nonlinear finite element modeling

Two-dimensional finite element models of the prototype building are developed in OpenSees simulation framework [41]. To evaluate the effect of butterfly-shaped fuse, two representations of the prototype building are constructed. The first model represents the original eccentrically braced frame (herein referred to as the EBF model), whereas the second model represents the braced frame equipped with butterfly fuses (herein referred to as the BF model). Figure 4 shows the schematic of the two models. The general configuration of both models uses elastic elements for beams, columns, and braces, since these components will not contribute to the inelastic action of the considered systems. The second-order effects of gravity frames are explicitly modeled using leaning columns. Each

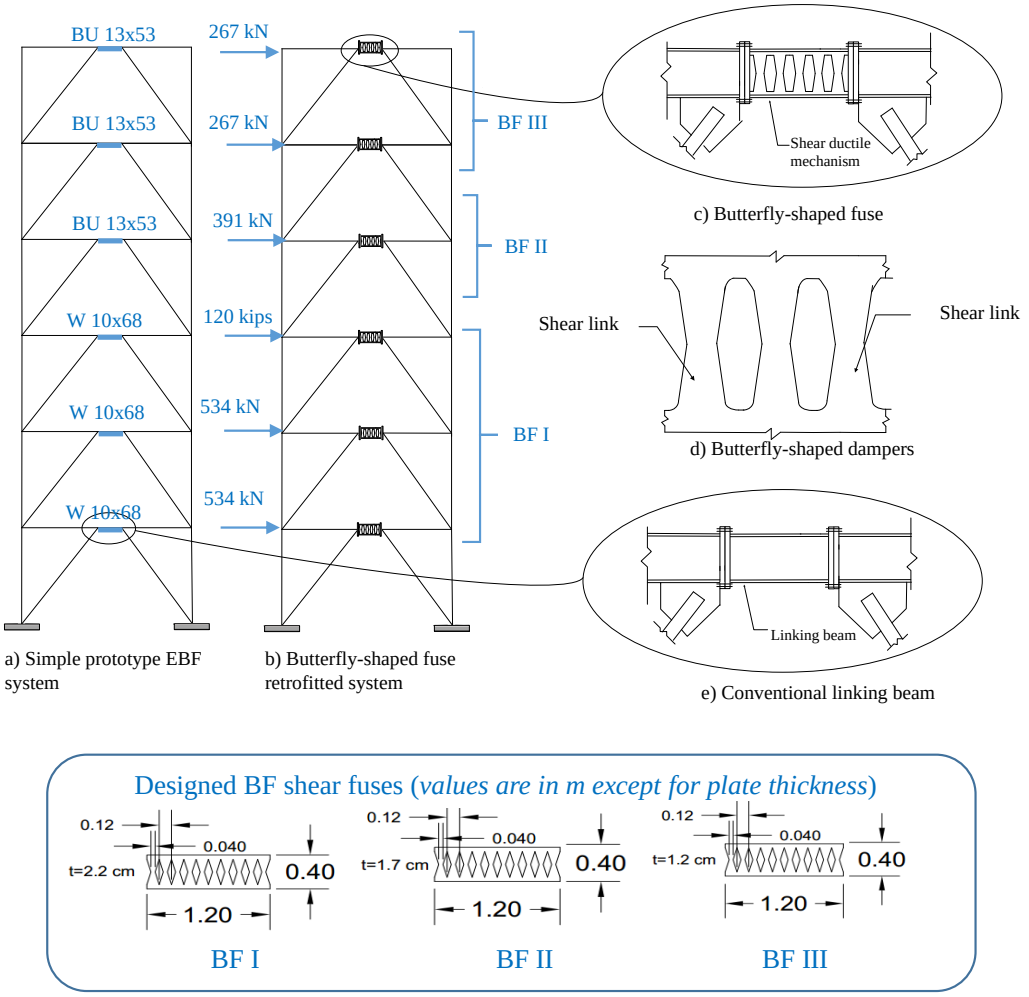

Fig. 3: Prototype buildings configuration and detailing

leaning column carries half of the weight of the interior gravity frames, and is connected to the main lateral-resisting frame through rigid links. In order to define damping in both numerical models, the Raleigh method is used to assign 2% critical damping ratios for the first two modes.

In the EBF model, the structural fuse, i.e. linking beam between braces, is expected to behave inelastically and hence, is modeled using an elastic element with plastic hinges at both ends. The plastic hinges are defined as shear springs using zero-length elements at the intersection of the fuse and braces in OpenSees. The hinges are modeled so that they will yield when the vertical demand of the system surpasses the shear strength of the EBF link. On the other hand, all the nonlinearity is expected to concentrate in butterfly fuses for the BF model. Therefore, the butterfly shear links are modeled with a series of displacement-based distributed plasticity elements (i.e. *dispBeamColumn*), which consider five integration points along the links' length. Each *dispBeamColumn* element is then discretized to varying fiber sections to consider the tapered shape of links. The top and bottom plates of the beam are modeled using *elasticBeamColumn* elements since their contribution to the inelastic action of fuses is negligible. The *Steel02* material is used to define steel fibers by Guiffre-Menegotto-Pinto Model with 248 MPa yield strength and a 0.0005 strain-hardening ratio.

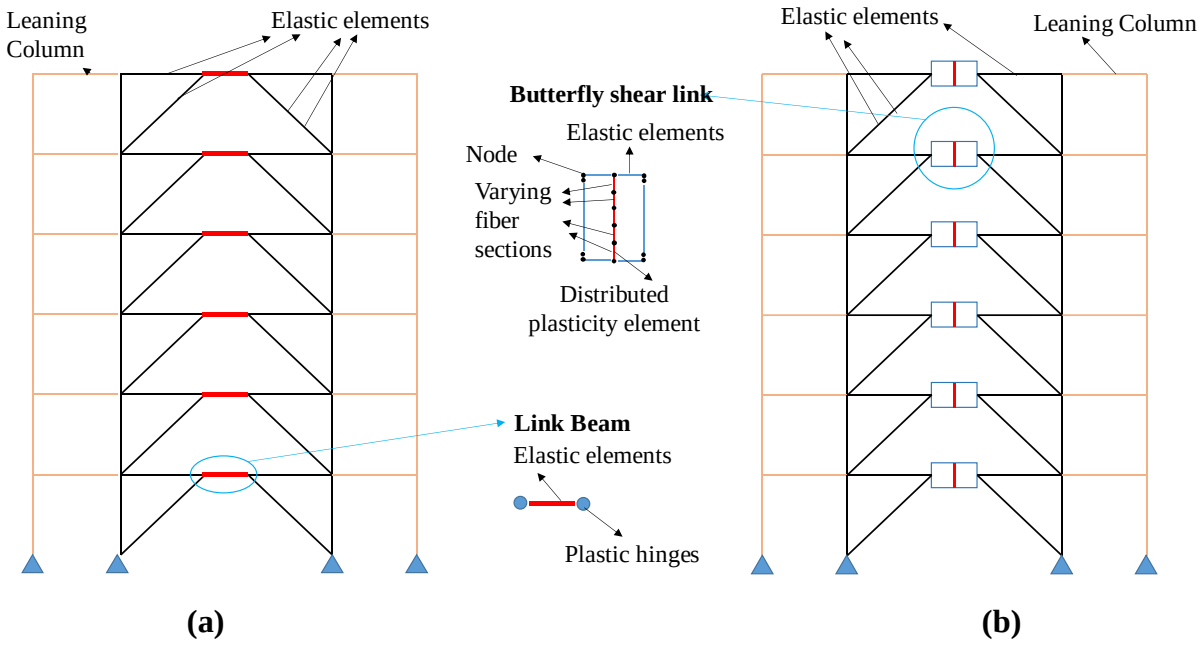

Fig. 4: Schematic representation of (a) EBF and (b) BF finite element configuration in OpenSees

2.3 Verification of numerical modeling

To verify the modeling approach of butterfly-shaped fuses, first, a detailed finite element model of the shear fuse is developed in ABAQUS finite element software and verified against experimental results provided previously by Aschheim and Halterman [24]. Using the same finite element model, the cyclic behavior of the butterfly-shaped fuse for the first story of the prototype building is captured and compared to the corresponding reduced-order OpenSees model to ensure that the results

The experimental study consists of an interior beam with five circular cut-outs with the top and the base beams made of TS14x10x5/8 and TS16x12x5/8, respectively. The beam is then modeled using solid elements with controlled hourglass and shear locking effect (*C3D20R* element in ABAQUS) to precisely capture the second-order behavior. Steel material is defined using a bi-linear stress-strain constitutive model with the yielding strength of 379 MPa, a strain-hardening modulus of 1.38 GPa, and an elastic modulus of 200 GPa. An initial imperfection of 1/250 of the beam's length is considered to simulate the first mode of buckling. Cyclic pushover analysis is performed on the numerical model using ATC 24 loading protocol and the results are compared in Figure 5.a. It is noted that the story shear force and drift of the FEM model are taken as 1.43 and 0.75 times of the beam shear and chord rotation based on experimental setting geometry, respectively. The difference between the average maximum strength values captured from the finite element model and experimental results is less than 5%. For example, the strength before and after buckling of the experimented beam is 76 kN and 57.4 kN, while the FEM model captured the strength at the same drift ratios with 73.2 kN and 52.7 kN, respectively.

The developed FEM model is then adjusted to represent diamond-shaped cut-outs of the butterfly-shaped fuse of the first story of the BF model. Similarly, a reduced-order model is developed in OpenSees following the approach described in the previous section and both models are subjected to AISC 341 loading protocol recommend for EBF systems experimental investigation[27,42]. As shown in Figure 5.b, the two models are in satisfactory agreement and represent a similar trace at both loading and unloading regions, where the average difference between cyclic results of the two models is less than 2%.

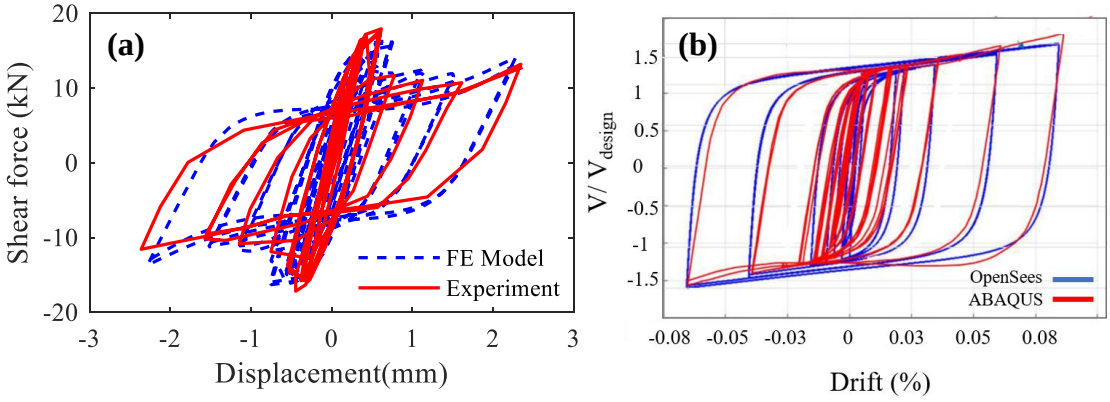

Fig. 5: Verification of the proposed butterfly-shaped fuse modeling: (a) comparison of cyclic pushover of butterfly-shaped shear fuse from FEM and experimental results (b) the cyclic results for OpenSees and ABAQUS models

3 Seismic performance assessment

In the previous sections, the analytical modeling of the original and retrofitted prototype building was discussed. In this section, incremental dynamic analysis is performed and the results are used to assess the seismic behavior of the original and retrofitted buildings from three different perspectives: (a) structure's fragility curves, (b) story-based fragilities and demand profiles, and (c) seismic demand hazard curves.

3.1 Incremental dynamic analysis

Incremental dynamic analysis (IDA) is performed to derive probabilistic estimates of structural response, where a suite of ground motion (GM) is successively scaled to increasing values of a given intensity measure (IM), and structure's response is recorded at each step by performing time-history analysis[43]. The standard FEMA P695 far-field record suite is used[44]. This suite includes 22 horizontal pairs of strong ground motions from earthquakes with magnitudes between 6.5 to 7.6 and distances larger than 10 Km, and has been widely used to perform IDA on both existing and new structural systems [39,45]. Two types of structural responses are recorded in terms of maximum inter-story drift (IDR_{max}) and peak floor acceleration (PFA) to quantify damages to structural and non-structural components.

The accuracy of IDA largely depends on the choice of GM intensity measure (IM) due to the inherent large record-to-record variability [46]. In this regard, IMs need to be efficient, i.e. are able to reduce variability in the estimation of response [47]. The IMs' efficiencies vary for different structural responses[48], hence two separate IMs of spectral acceleration at the first mode, $S_a(T_1)$, and peak ground acceleration (PGA) are adopted for IDR_{max} and PFA, respectively. Separate IDAs are performed for each selected IM, at which each IM is scaled up to 4 g at 0.1 g intervals to cover a complete spectrum of structure's response from elastic to collapse. At each IM level, acceleration and drift demands are recorded at all story levels for post-processing. Figure 6 Shows the IDA curves of the two systems. To represent IDA results uncertainty, 16th and 84th percentile curves corresponding to mean plus/minus one standard deviation are shown.

As shown in Figure 6.a, the median values of Sa for a given IDR_{max} level is higher for the BF building comparing to the EBF. For example, the median Sa values of the building equipped with BF fuses are 60.4% and 48.7% larger than the EBF system at 2% and 10% drift values, respectively. This observation indicates that under larger shaking intensities, the BF system maintains relatively smaller drift values, and hence can better dissipate the seismic forces. Figure 6.b shows that BF

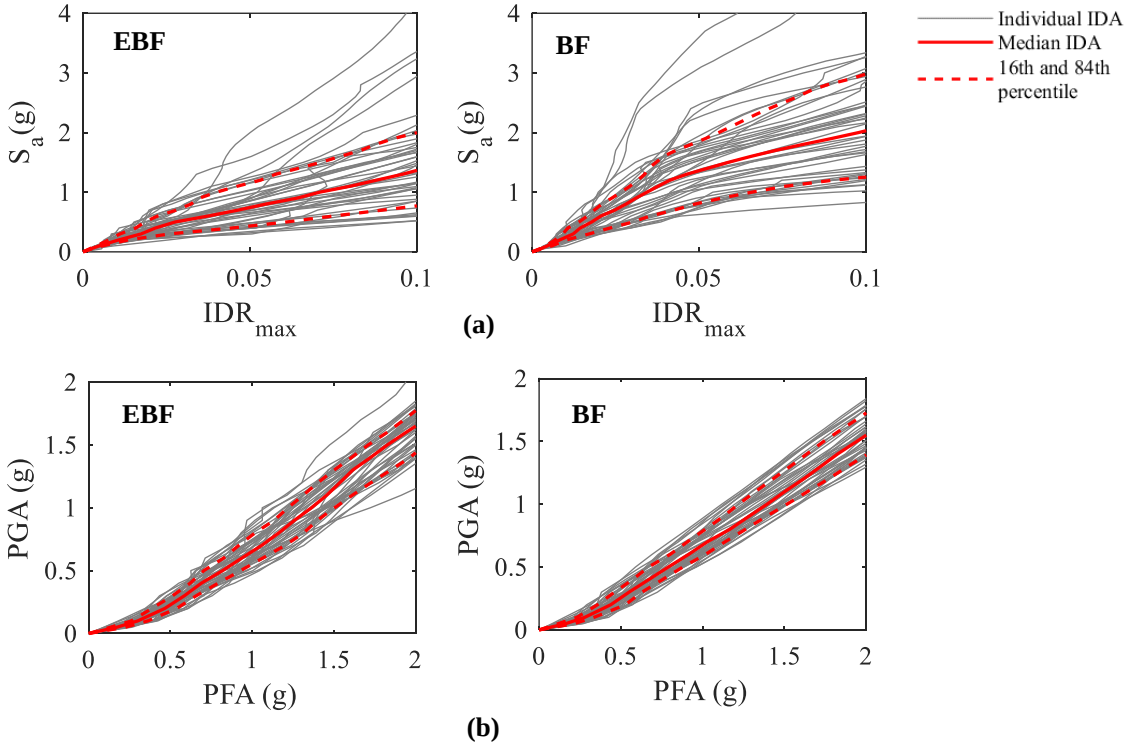

Fig. 6: Comparison of IDA curves of drift- and acceleration-related responses of BF and EBF system

fuses have a smaller effect on PFA comparing to IDR_{max}, and both BF and EBF models have very close median PFA values. In addition, the BF system shows better performance at lower PFA value. For example, the median PGA value of the building retrofitted with BF fuse is 11.9% larger than the EBF system at PFA value of 0.5g, whereas the difference between two buildings reduces to 6.2% for a PFA value of 2g. It should also be noted that the uncertainty in PFA estimation is significantly lower than IDR_{max} for both buildings and IDA curves show linear trends.

3.2 Global fragility estimation

Analytical seismic fragilities are conditional cumulative distribution probabilities that relate ground motion intensity to the structural damage level, commonly measured in terms of global limit states. Following a lognormal assumption, the probability of exceeding a given level of edp when the expected ground motions have an intensity level of im is defined as follows:

$$P(EDP > edo|IM = im) = \Phi(\frac{\ln(\frac{x}{\theta})}{\beta}) \tag{1}$$

where Φ is the standard normal cumulative distribution and θ and β are the median and standard deviation of fragility functions that are estimated from the IDA. A statistical method is then implemented to estimate θ and β in the presence of the ground motion record-to-record variability. An efficient method to construct fragility curves from IDA results is the method of moments [49]. In this method, the resulting distribution of the fragility function should have the same statistical moments (e.g. median and standard deviation) as the moments of the IDA results. Subsequently, the number

of GMs that exceeds the given limit state is calculated at each IM value, and the parameters of fragility function are derived as follows:

$$\ln(\hat{\theta}) = \frac{1}{n}\Sigma_{i=1}^{n} \ln IM_i$$
$$\ln(\hat{\beta}) = \sqrt{\frac{1}{n-1}\Sigma_{i=1}^{n}(\ln IM_i - \frac{1}{n}\Sigma_{i=1}^{n} \ln IM_i)^2} \quad (2)$$

Fragility curves are estimated for four different limit states of slight, moderate, extensive, and complete damage states based on the HAZUS guideline [50]. For drift response, IDR_{max} of 0.3%, 0.67%, 2%, and 5% are respectively adopted for the aforementioned limit states of braced steel frames. For acceleration-based fragilities, PFA values of 0.3g, 0.6g, 1.2 g, and 2.4 g are adopted for the corresponding limit states [50].

Figure 7 shows the fragility curves of the two considered buildings. The median and dispersion values of all fragility curves are provided in Table 1. Overall, the building with BF shear fuses exceeds drift-related damage states at higher Sa values, and the difference increases for higher damage states corresponding to near-collapse limit states.

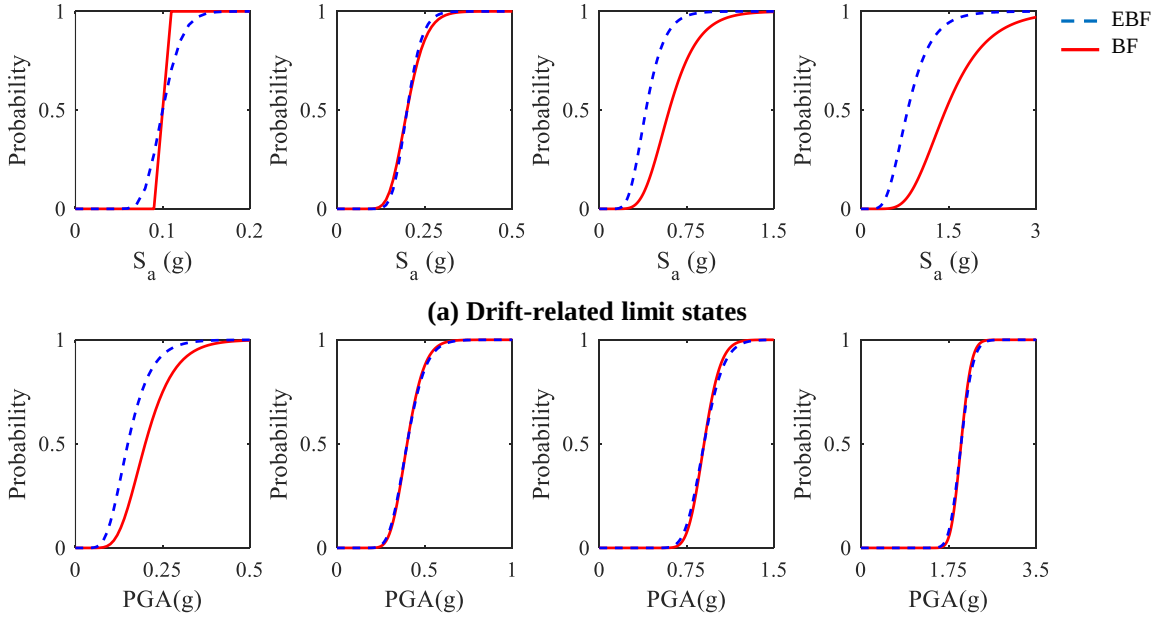

(a) Drift-related limit states

(b) Acceleration-related limit states

Fig. 7: Comparative fragility curves of EBF and BF systems under (i) slight, (ii) moderate, (iii) extensive, and (iv) complete damage states.

Table 1: Median and standard deviation of structures' fragility curves

Building	Slight		Moderate		Extensive		Complete	
	median	std	median	std	median	std	median	std
	IDR max							
EBF	0.1	0.18	0.2	0.17	0.4	0.31	0.8	0.4
BF	0.1	0.01	0.2	0.21	0.6	0.33	1.45	0.38
	PFA							
EBF	0.15	0.35	0.4	0.21	0.9	0.15	2.0	0.09
BF	0.2	0.33	0.4	0.19	0.9	0.13	2.0	0.08

The median Sa value of the BF system exceeding extensive damage state is 50% more than the EBF system, whereas, for the complete damage state, the difference increases to 81.2%. It should be noted that at lower damage states corresponding to slight and moderate, the difference between two systems is negligible. Regarding acceleration-based limit states, two systems show similar performance at moderate, extensive and complete damage states, however, the BF system has a lower probability to exceed the slight damage state for a given PGA value. The median PGA of the BF system exceeding the slight damage state is 33.3% larger than the EBF system.

To summarize, BF fuses significantly improve the structure's seismic performance at larger drift demands, while maintaining the same acceleration response as the EBF. For the slight damage state, the BF system is more effective to reduce PFA compared to IDR_{max} due to additional system stiffness that the fuses provided. Lastly, the BF system shows smaller dispersion on average for both drift- and acceleration-based fragilities (17.3% and 9.9%, respectively) compared to the EBF system. The dispersion in response stems from two different sources: (a) GM input (b) structure's dynamic characteristic. Dispersion due to GM input is reflected in IM's efficiency to capture the structure's response at the range of recorded response, whereas dispersion due to dynamic properties is related material nonlinearity and structural damage. Since the same ground motion suite and IM is used for both models, it can be concluded that the BF shear fuses are effective to postpone system yielding and limit inelastic behavior to more severe limit states, which result in lower dispersion at less severe damage states.

3.3 Impact of butterfly-shaped fuses on story mechanism

In this section, the impact of butterfly-shaped fuses on story mechanisms is investigated using story-specific fragility curves and heightwise drift and acceleration profiles. Story-specific fragilities are derived from the maximum values of each floor's drift and acceleration responses, following the same approach described in the previous section for global responses. Figure 8 shows the derived story-specific fragilities, where the thickness of curves increases with the story number, i.e. the thickest line belongs to the sixth story. Figure 8 shows that the difference between story-specific fragilities of two systems is larger for story drifts comparing to story acceleration responses, indicating that butterfly-shaped fuses have a larger impact on story drift demand. Table 2 provides the story fragilities' median and dispersion values of the two systems under the considered limit states.

Figure 8.a compares the drift-based story fragilities of the two studied buildings. overall, the butterfly-shaped fuses have a more substantial effect on lower stories of the prototype building which experience larger drift demand. In addition, the impact of butterfly-shaped fuses is shown to be more pronounced on the higher damage states. The story fragility curves of the BF system, particularly the first three stories, are closely spaced at each damage state and have less dispersion compared to the EBF system. This confirms prior observations that butterfly-shaped fuses result in a more uniform story response. Since the first three stories are equipped with butterfly-shaped shear fuses with larger ductility capacity (group I in Figure 3), they do not exhibit significant yielding under lower damage states, which led to the lower dispersion. While the fragilities of several BF stories exceed lower damage states at a lower median Sa value, all stories of the BF system exceed more severe damage states at a larger median Sa value than the EBF system. For example, the median Sa values of the second and third stories of the BF system exceed the slight damage state at 50% and 33.3% smaller values than the EBF system. On the other hand, the first to sixth story of the BF system exceed complete the damage state at 81.3%, 75%, 47.4%, 23.9%,11.1%, and 33.9% larger median Sa values than the same stories of the EBF system, respectively.

Figure 8.b compares acceleration-based story fragility curves. It is shown that except for the first story, other stories' fragilities do not vary significantly and the difference decreases at higher damage states. In contrast to drift-based story fragilities, all the acceleration-based fragilities of the BF system's upper stories exceed higher damage states at a smaller median PGA value, but the

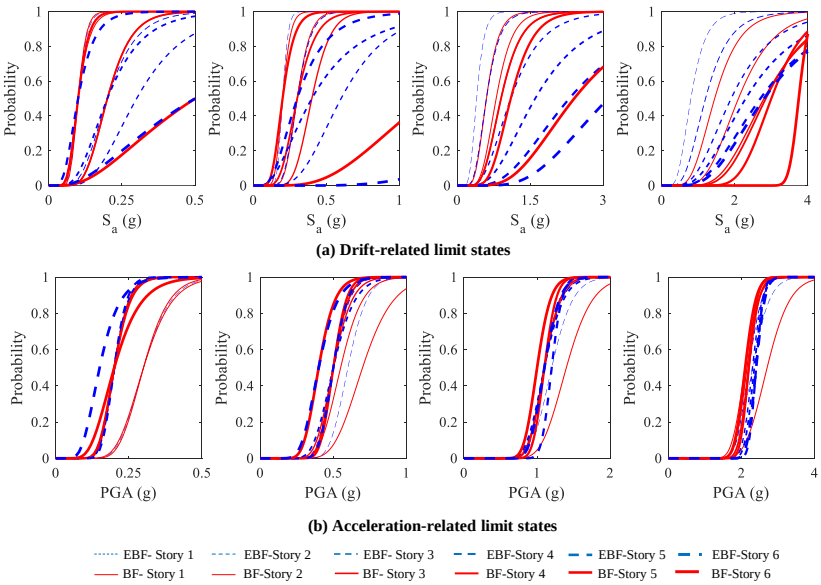

Fig. 8: Comparison of story-specific fragilities of two systems under (i) slight, (ii) moderate, (iii) extensive, and (i) complete damage states.

Table 2: Median and standard deviation of story-specific fragility curves

Building	Story No.	Slight		Moderate		Extensive		Complete	
		median	std	median	std	median	std	median	std
		Story drift							
EBF	1	0.1	0.24	0.2	0.15	0.4	0.31	0.8	0.4
	2	0.2	0.39	0.3	0.25	0.6	0.36	1.2	0.43
	3	0.3	0.45	0.6	0.42	1.1	0.46	1.9	0.48
	4	0.2	0.47	0.4	0.66	1.6	0.51	2.3	0.51
	5	0.1	0.44	0.3	0.53	2.3	0.53	2.7	0.51
	6	0.5	0.83	2.35	0.47	3.1	0.46	2.8	0.48
BF	1	0.1	0.22	0.2	0.22	0.6	0.33	1.45	0.38
	2	0.1	0.32	0.3	0.24	0.8	0.33	2.1	0.37
	3	0.2	0.33	0.4	0.25	0.9	0.36	2.8	0.37
	4	0.2	0.33	0.3	0.33	0.9	0.36	2.85	0.33
	5	0.1	0.28	0.2	0.32	1.1	0.33	3	0.24
	6	0.5	0.75	1.2	0.52	2.4	0.47	3.75	0.06
		Story acceleration							
EBF	1	0.3	0.24	0.6	0.17	1.2	0.19	2.3	0.16
	2	0.2	0.22	0.5	0.16	1.1	0.17	2.2	0.13
	3	0.2	0.21	0.5	0.17	1.1	0.15	2.3	0.1
	4	0.2	0.19	0.5	0.23	1.1	0.19	2.35	0.09
	5	0.2	0.17	0.5	0.16	1.2	0.09	2.4	0.07
	6	0.15	0.35	0.4	0.25	1.1	0.15	2.4	0.08
BF	1	0.3	0.26	0.7	0.23	1.4	0.2	2.7	0.18
	2	0.3	0.23	0.55	0.21	1.1	0.17	2.1	0.14
	3	0.2	0.22	0.5	0.2	1	0.15	2.15	0.12
	4	0.2	0.2	0.5	0.16	1.1	0.16	2.2	0.1
	5	0.2	0.22	0.5	0.14	1.1	0.12	2.2	0.09
	6	0.2	0.35	0.4	0.22	1	0.15	2.1	0.11

difference is not significant. On the other hand, the first story of the BF system exceeds complete damage state at a median PGA value larger than all other stories of both systems.

For example, the second and sixth stories of the BF system exceed the slight damage at a 50% and 33.3% larger median PGA value compared to the EBF system, whereas the rest of the stories show similar median PGA values. On the contrary, the first story of the BF system exceeds the complete damage state at a 17.4% larger PGA value than the EBF system, whereas all other stories of the BF system exceed the same damage state at smaller median PGA values.

To further investigate the stories' responses, Figure 9 compares drift and acceleration profiles at the design basis earthquake (DBE) and maximum considered earthquake (MCE) levels. DBE and MCE levels are defined as earthquakes with 10% and 2% exceedance probability in 50years at the site, respectively. Since the period of the original and retrofitted models are very close (1.33 s versus 1.28 s for BF and EBF systems, respectively), they undergo similar Sa demands under DBE and MCE level. Therefore, it provides a comparable basis to assess both models under low and high seismic shaking intensities. As shown in Figure 9.a and 9.b, the BF system shows smaller median drift values for the first two stories and slightly larger drift values for top stories at both DBE and MCE levels. Figures 9.c and 9.d show that the acceleration profiles of the two systems are quite similar for the DBE level. In addition, the BF system yields smaller floor acceleration at the second story and slightly larger acceleration at top stories under MCE.

An important observation is that while the EBF system shows large drift accumulation at the first story, particularly at MCE level, butterfly-shaped fuses effectively reduce the excessive drift concentration. As discussed by Simpson and Mahin [9], conventional steel braced frames tend to form weak story under seismic loading due to degradation of the buckled braces' strength, causing a relatively weaker story comparing to stories with braces that sustained smaller inelastic deformation.

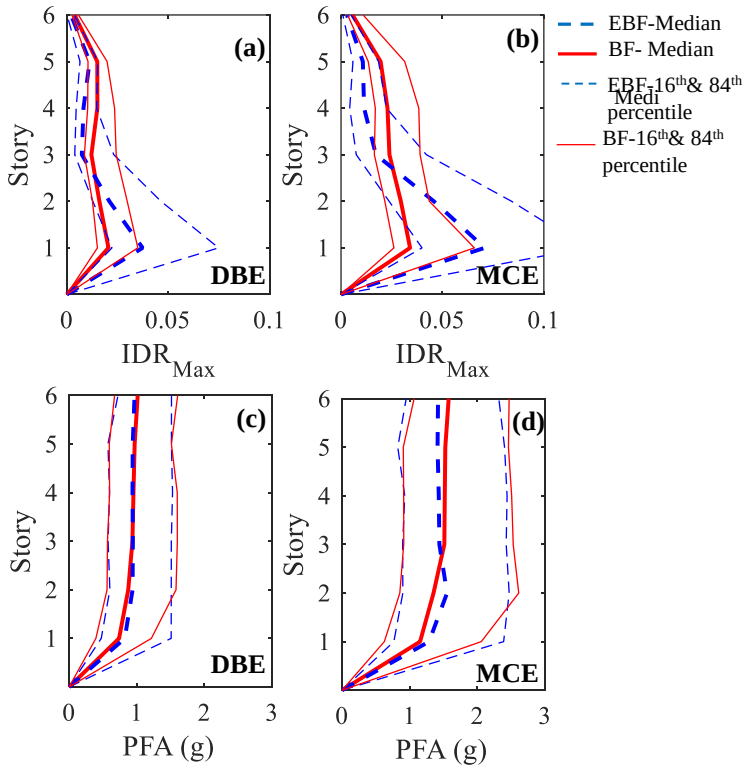

Fig. 9: Drift and acceleration profile of considered systems

Since butterfly-shaped shear fuses have larger dissipation capacity and ductility than a conventional EBF link, they can better absorb the lateral load through excessive yielding, reducing the demand on the rest of structural components, and subsequently limiting stories' peak drifts through redistribution of lateral forces in the entire frame. Therefore, this observation suggests that the BF fuse can be used to prevent weak story formation in multi-story buildings.

3.4 Seismic demand hazard curve

Seismic demand hazard curves represent the mean annual frequency of exceeding different EDP levels and are unique for a given structure at a site [51]. Seismic demand hazard curves are derived by integrating the product of the structure's vulnerability (in terms of fragility curve) and the site's hazard (in terms of IM hazard curve) as follows:

$$\lambda(EDP) = \int_{IM} G(EDP|IM).|\frac{d\lambda(IM)}{dIM}|dIM \tag{3}$$

Where λ is the mean annual frequency (MAF) of exceeding a variable and G(EDP—IM) denotes the probability of exceeding EDP for a given IM. The IM hazard curves (i.e. $\lambda(IM)$) are derived from the USGS unified hazard tool (https://earthquake.usgs.gov/hazards/interactive/) for the buildings' site and interpolated based on the fundamental period of each building.

Figure 10 shows the seismic demand hazard curves of the BF and EBF systems and Table 3 provides the MAF values at the considered limit states. Consistent with previous sections, the BF system has a lower MAF of IDR_{max} compared to the EBF system, and the difference increases at larger drift demands. For example, MAF of exceeding the slight damage state of the BF system is 12.57% smaller than the EBF, whereas MAF of the complete damage for the BF system is 76.9% smaller than the EBF system. In addition, MAF can be used to calculate the probability of exceeding a limit state in 50 years as follows:

$$P_{50-year} = 1 - \exp^{-\lambda t} \tag{4}$$

Using Eq.4, the probabilities of exceeding the drift-related complete damage state in 50 years are 7% and 2% for the EBF and BF systems. This indicates that butterfly-shaped fuses reduce the complete damage risk to almost one-fourth of the EBF system. Since the structure's inelastic deformation (i.e. drift at higher damage states) is related to the system's ductility [39,52,53], it can be concluded that shear fuses' substantial ductility led to the observed reduction in MAF of IDR_{max}.

As shown in Table 3 and Figure 10.b, the difference between MAF of PFA for the two systems is negligible. Previous studies have shown that floor acceleration response is proportional to the building's stiffness [54,55]. Since butterfly-shaped shear fuses do not provide significant additional stiffness for the whole system, comparing to the boundary elements' stiffnesses, it is expected that their impact on floor acceleration to be trivial. It should be noted that MAF of exceeding acceleration-based damage states are notably smaller than drift-based ones for both systems, indicating that both the EBF and butterfly-shaped fuse can effectively reduce floor acceleration demands. For example, the probability of exceeding the complete acceleration-related damage state is 0.4% for both systems.

4 Story-based loss assessment

In Section 3, the original and retrofitted buildings were compared from global and story-based damage perspectives. In this section, a story-based loss assessment is performed to compare the original and retrofitted buildings from an economic perspective. The story-based approach simplifies the seismic loss calculations by lumping building components to assembly types (e.g. structural, non-structural) and corresponding EDP; hence, it requires less information compared to the more rigorous

Table 3: MAF (x10-3) of two systems under considered performance levels

Building	Slight	Moderate	Extensive	Complete
	IDR_{max}			
EBF	52.75	27.98	4.89	1.39
BF	46.12	20.77	2.22	0.32
	PFA			
EBF	22.49	4.56	0.88	0.09
BF	13.88	4.24	0.79	0.08

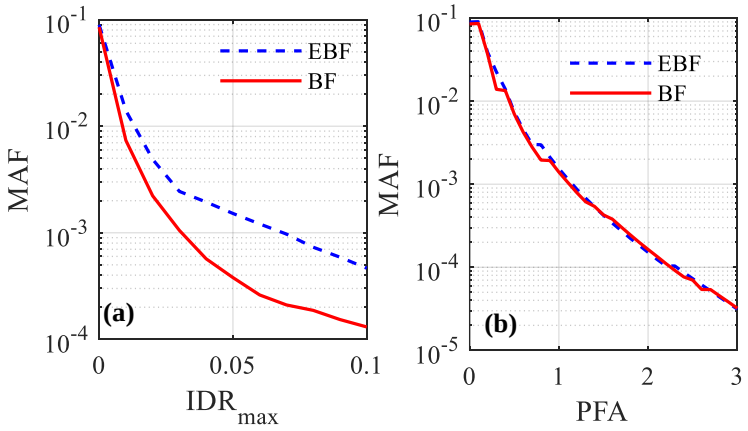

Fig. 10: Comparison of seismic demand hazard curve of (a) IDR_{max} and (b)PFA of two systems

component-based approach such as the one outlined in FEMA P58 framework [56,57,58]. In this study, the seismic loss is defined in terms of direct repair cost, and other sources of economic loss due to occupants' injury, fatality, relocation, and the indirect economic costs related to the interruptions are not included [59]. Therefore, the results are provided in a comparative basis, focusing on the costs associated with the structural and non-structural performance from a global perspective, rather than a precise estimation of all the possible losses during the structure's life cycle. Following Ramirez et al [60], the expected total loss (LT) conditioned on the ground motion intensity level, is treated separately for collapse (C) and non-collapse (NC) cases as follows:

$$E(L_T|IM) = E(L_{NC}|NC, IM)(1 - P(C|IM)) + E(L_C|C, IM)P(C|IM) \tag{5}$$

where E(X—Y) is the expected value of random variable X conditioned on Y, and P(X) shows the probability of random variable X. The non-collapse loss is then disaggregated to structural (L_S), drift-sensitive non-structural ($L_{NS,DS}$), and acceleration-sensitive non-structural assemblies ($L_{NS,AS}$) as follows:

$$E(L_{NC}|NC, IM) = E(L_S|NC, IM) + E(L_{NS,DS}|NC, IM) + E(L_{NS,AS}|NC, IM) \tag{6}$$

The expected loss of each assembly is calculated by summation over a discrete number of damage states following the HAZUS guideline [50] as follows:

$$E(L_i|NC, IM) = \Sigma_{i=1}^{m} \int E(repair\ cost|DS_i)P(DS_i|EDP)P(EDP|IM)dEDP \tag{7}$$

where $P(DS_i|EDP)$denotes the probability of exceeding damage state i (DS_i) and is calculated as follows:

$$P(DS_i|EDP) = \begin{cases} 1 - P(EDP > edp = DS_i|IM), & i = 0 \\ P(EDP > edp = DS_{i-1}|IM) - P(EDP > edp = DS_i|IM), & 1 \leq i < n \\ 1 - P(EDP > edp = DS_i|IM), & i = n \end{cases} \quad (8)$$

Figure 11 compares the normalized vulnerability curves (i.e. expected loss in terms of building replacement in percent) for both considered systems. It should be noted that the initial cost of the BF system is conservatively assumed to be 5% more than the original EBF system due to additional fabrication, detailing, and placement of fuses. Figures 11.a to 11.c show the loss conditioned on IM levels at which collapse does not happen (i.e. L_S,$L_{NS,DS}$ and $L_{NS,AS}$, respectively), whereas Figure 11.d shows the total economic loss of all assemblies considering both collapse and non-collapse cases(i.e. L_T). It should be noted that collapse is defined when the building reaches an IDR_{max} value of 10%, following previous recommendations for steel frames [61].

As shown in Figure 11.a and 11.b, losses due to structural and drift-sensitive non-structural assemblies grow at a slower rate for the BF system at higher IM levels. In addition, the peak losses of structural and drift-sensitive non-structural assemblies of the BF system occur at a larger IM value. For example, at the DBE and MCE level, the BF system experiences a 44.8% and 57.1% smaller structural loss compared to the EBF system, respectively, whereas the drift-sensitive non-structural loss of BF system is 56.6% and 35.3% smaller than the EBF system for the same hazard levels.

Figure 11.c shows that the losses associated with acceleration-sensitive non-structural assemblies are quite similar between the two systems, however, the BF system shows a slightly higher loss at

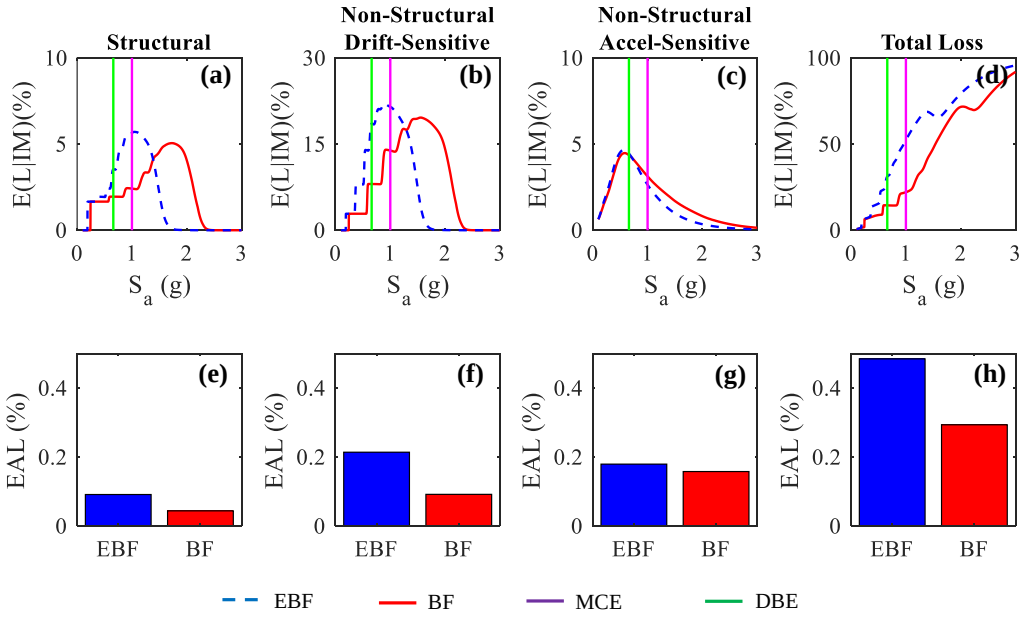

Fig. 11: Comparison of economic vulnerability and expected annual loss of two systems: Vulnerability curves excluding collapse loss for (a) structural assemblies, (b) drift sensitive non-structural assemblies, (c) acceleration-sensitive non-structural assemblies and (d) total loss of all assemblies including collapse. Figures (e) to (f) show the expected annual loss for each of the aforementioned cases by integrating each corresponding vulnerability curve with the site hazard curve.

larger IM values (i.e. Sa larger than 0.9 g). Figure 11.d shows that the total loss of both systems varies linearly with the IM level. Although losses due to non-collapse cases decrease for larger IM values, the contribution of collapse loss increases. The trade-off between these two sources of loss results in a linear increase due to the larger magnitude of collapse loss. Furthermore, the BF system has a significantly smaller total loss than the EBF system. At the DBE and MCE hazard levels shown in Figure 11.d, the total loss of the BF system is 45.9% and 34.7% smaller than the EBF system, respectively.

Similar to the seismic demand hazard curve, $E(L_i|IM)$ can be integrated over the site's hazard to derive expected annual loss (EAL) as follows:

$$\lambda(L_i) = \int_{IM} E(L_i|IM).|\frac{d\lambda(IM)}{dIM}|dIM \tag{9}$$

The advantage of the EAL metric over vulnerability curves is that it accounts for all possible site hazard levels, hence the impact of more frequent seismic events is emphasized [62]. Figure 11.e to 11.h show the expected annual loss calculated from Eq.9 for each of the corresponding vulnerability curves related to Figures 11.a to 11.d, respectively.

As shown in Figures 11.e to 11.h, the BF system shows smaller EAL for all assemblies, where the cumulative non-collapse losses of the EBF and BF systems are 0.48% and 0.29% of prototype buildings replacement cost, respectively. In addition, while the drift-sensitive non-structural assembly dominates the total EAL of the EBF building (39.9% of total EAL for EBF), acceleration-sensitive non-structural assembly dominates the total EAL of the BF system (51.5% of total EAL for BF). This is mainly because butterfly-shaped fuses reduce drift demands and their consequent impact on the total building loss. Lastly, while the BF system shows a higher loss value for non-structural acceleration-sensitive assemblies at larger IM values, the EAL of this particular assembly is still 11.9% smaller than that of the EBF system. This indicates that acceleration-sensitive losses are governed by more frequent earthquakes which push the structure to less severe damage states, and as a result, the BF system outperforms the EBF system.

5 Conclusion

This paper studies the impact of butterfly-shaped (BF) fuses on the seismic performance and earthquake-induced loss of a multi-story steel eccentrically braced (EBF) building. Two sets of non-linear finite element models are developed for the original and retrofitted buildings, where a novel reduced-order modeling approach is proposed to simulate BF fuses. Incremental dynamic analysis is conducted and structures' global performance is evaluated using drift- and acceleration-based fragility and seismic demand hazard curves. In addition, story-based fragilities are derived to scrutinize the effect of BF fuses on the story mechanism under different shaking intensities. Subsequently, a simplified story-based loss methodology was adopted to compare vulnerability curves and expected annual loss of different building assemblies. The followings summarize the main findings of this paper:

1. Based on fragility curves results, building with BF fuses has a lower probability of exceeding drift-related damage states, and the difference increases at more severe states. In particular, the median fragility of the BF system is 81.2% higher than the EBF system for the drift-based complete damage state. Conversely, both BF and EBF systems show similar probabilities of exceeding acceleration-based limit states at higher damage states, whereas the BF system slightly outperforms EBF at the slight damage state.
2. Story-based fragility curves show that the impact of BF fuses is more pronounced on the lower stories, which undergo larger seismic drift demand. In contrast, except for the first story, acceleration-based story fragilities do not vary significantly and the difference decreases at higher damage states.

3. The studied butterfly-shaped fuses prevent weak story formation observed at the first story of the EBF system under the MCE hazard level. In addition, at both DBE and MCE levels, the BF system shows smaller median drift values than the EBF system for the two bottom stories.
4. Based on the drift hazard curves, the mean annual frequency of exceeding the complete damage state of the BF and EBF systems are 13.9x10-4 and 3.2x10-4, respectively. Therefore, BF fuses reduce the probability of complete damage in 50 years by a factor of 4.
5. The structure equipped with butterfly-shaped fuses has 51.9%, 57.1%, and 11.9% lower expected annual loss for structural, drift-sensitive, and acceleration-sensitive non-structural assemblies that the original building. The total expected annual losses of the EBF and BF system are 0.56% and 0.31% of the building replacement.
6. While losses due to repairing drift-sensitive non-structural assembly govern the total loss of the EBF system, butterfly-shaped fuses effectively reduce all drift-related losses, resulting in acceleration-sensitive non-structural assemblies to govern the total expected loss of the BF system.

The results of this study support utilizing BF shear fuses to upgrade the seismic performance of multi-story steel buildings, particularly to mitigate risks of exceeding higher damage states. However, the findings of this study are limited to the geometry of the prototype building, location, and seismic detailing. Therefore, further research is required to investigate the effect of building taxonomy (e.g. different geometry, lateral-resisting systems, etc.) and site's seismicity effects on BF fuses performance. From a seismic design perspective, additional research is needed to streamline the butterfly-shaped fuses' design process for achieving a desired level of performance in buildings equipped with these devices. Lastly, since the proposed modeling approach can readily be implemented in community resiliency-based evaluation, future studies are useful to compare butterfly-shaped shear fuses with other retrofitting strategies for upgrading existing steel multi-story buildings in highly seismic zones.

Acknowledgement

The computational models are developed based upon the work supported by the National Science Foundation under Grant No. CMMI-1453960. Any opinions, findings, and conclusions or recommendations expressed in this material are those of the authors and do not necessarily reflect the views of the National Science Foundation or other sponsors. The authors also acknowledge Dr. Matthew R. Eatherton for providing technical support that has contributed to the establishments of the computational models.

References

1. Laurens M Bouwer. Projections of future extreme weather losses under changes in climate and exposure. *Risk Analysis*, 33(5):915–930, 2013.
2. Hessel C Winsemius, Jeroen CJH Aerts, Ludovicus PH Van Beek, Marc FP Bierkens, Arno Bouwman, Brenden Jongman, Jaap CJ Kwadijk, Willem Ligtvoet, Paul L Lucas, Detlef P Van Vuuren, et al. Global drivers of future river flood risk. *Nature Climate Change*, 6(4):381–385, 2016.
3. Maria Koliou, John van de Lindt, Bruce Ellingwood, Maria K Dillard, Harvey Cutler, and Therese P McAllister. A critical appraisal of community resilience studies: Progress and challenges. Technical report, 2018.
4. Hassan Masoomi and John W van de Lindt. Community-resilience-based design of the built environment. *ASCE-ASME Journal of Risk and Uncertainty in Engineering Systems, Part A: Civil Engineering*, 5(1):04018044, 2019.
5. Mark Grigorian, Abdolreza S Moghadam, Hadiseh Mohammadi, and Mozhgan Kamizi. Methodology for developing earthquake-resilient structures. *The Structural Design of Tall and Special Buildings*, 28(2):e1571, 2019.

6. Omar Kammouh, Stefano Silvestri, Michele Palermo, and Gian Paolo Cimellaro. Performance-based seismic design of multistory frame structures equipped with crescent-shaped brace. *Structural Control and Health Monitoring*, 25(2):e2079, 2018.
7. Michele Palermo, Luca Pieraccini, Antoine Dib, Stefano Silvestri, and Tomaso Trombetti. Experimental tests on crescent shaped braces hysteretic devices. *Engineering Structures*, 144:185–200, 2017.
8. Michele Palermo, Vittoria Laghi, Giada Gasparini, and Tomaso Trombetti. Coupled response of frame structures connected to a strongback. *Journal of Structural Engineering*, 144(9):04018148, 2018.
9. Barbara G Simpson and Stephen A Mahin. Experimental and numerical investigation of strongback braced frame system to mitigate weak story behavior. *Journal of Structural Engineering*, 144(2):04017211, 2018.
10. Ou Zhao, Barbara Rossi, Leroy Gardner, and Ben Young. Experimental and numerical studies of ferritic stainless steel tubular cross sections under combined compression and bending. *Journal of Structural Engineering*, 142(2):04015110, 2016.
11. Mojtaba Aliasghar-Mamaghani and Alireza Khaloo. Seismic behavior of concrete moment frame reinforced with gfrp bars. *Composites Part B: Engineering*, 163:324–338, 2019.
12. Saeid Tarfan, Mehdi Banazadeh, and Mohsen Zaker Esteghamati. Probabilistic seismic assessment of non-ductile rc buildings retrofitted using pre-tensioned aramid fiber reinforced polymer belts. *Composite Structures*, 208:865–878, 2019.
13. Matthew S Speicher, Reginald DesRoches, and Roberto T Leon. Investigation of an articulated quadrilateral bracing system utilizing shape memory alloys. *Journal of Constructional Steel Research*, 130:65–78, 2017.
14. Amin Moghadam, HE Estekanchi, and M Yekrangnia. Evaluation of pr steel frame connection with torsional plate and its optimal placement. *Scientia Iranica. Transaction A, Civil Engineering*, 25(3):1025–1038, 2018.
15. Hua Huang, Fantao Zhang, Wei Zhang, Mengxue Guo, Shota Urushadze, and Guochao Wu. Numerical analysis of self-centering energy dissipation brace with arc steel plate for seismic resistance. *Soil Dynamics and Earthquake Engineering*, 125:105751, 2019.
16. MH Mehrabi, Zainah Ibrahim, SS Ghodsi, and Meldi Suhatril. Seismic characteristics of x-cable braced frames bundled with a pre-compressed spring. *Soil Dynamics and Earthquake Engineering*, 116:732–746, 2019.
17. Yanxia Zhang, Quangang Li, Yan Zhuge, Anran Liu, and Wenzhan Zhao. Experimental study on spatial prefabricated self-centering steel frame with beam-column connections containing bolted web friction devices. *Engineering Structures*, 195:1–21, 2019.
18. MG Gray, C Christopoulos, and JA Packer. Cast steel yielding fuse for concentrically braced frames. In *Proceedings of the 9th US national and 10th Canadian conference on earthquake engineering*, volume 9. Earthquake Engineering Research Institute and the Canadian Association for ..., 2010.
19. Zhipeng Zhai, Wei Guo, Yaozhuang Li, Zhiwu Yu, Hongpeng Cao, and Dan Bu. An improved performance-based plastic design method for seismic resilient fused high-rise buildings. *Engineering Structures*, 199:109650, 2019.
20. Yang Liu, Zixiong Guo, Xiaojuan Liu, Rachel Chicchi, and Bahram Shahrooz. An innovative resilient rocking column with replaceable steel slit dampers: Experimental program on seismic performance. *Engineering Structures*, 183:830–840, 2019.
21. Tianxiang Li, TY Yang, and Genshu Tong. Performance-based plastic design and collapse assessment of diagrid structure fused with shear link. *The Structural Design of Tall and Special Buildings*, 28(6):e1589, 2019.
22. Shahrokh Shoeibi, Mohammad Ali Kafi, and Majid Gholhaki. New performance-based seismic design method for structures with structural fuse system. *Engineering Structures*, 132:745–760, 2017.
23. Toko Hitaka and Chiaki Matsui. Experimental study on steel shear wall with slits. *Journal of Structural Engineering*, 129(5):586–595, 2003.
24. M Aschheim and A Halterman. Reduced web section beams, phase one: Experimental findings and design implications. In *7th US national conference on earthquake engineering, Boston, Massachusetts*, 2002.
25. Myoungsu Shin, Seung-Pil Kim, Arne Halterman, and Mark Aschheim. Seismic toughness and failure mechanisms of reduced web-section beams: Phase 2 tests. *Engineering Structures*, 141:607–623, 2017.
26. G Luth, H Krawinkler, B McDonald, and M Park. Usc school of cinema: An example of reparable performance based design. In *Proceedings of the 77th Annual Structural Engineers Association of California (SEAOC) Convention, Sacramento, CA, USA*, pages 23–27, 2008.

27. Xiang Ma, Eric Borchers, Alex Pena, Helmut Krawinkler, and G Deierlein. Design and behavior of steel shear plates with openings as energy-dissipating fuses. *John A. Blume Earthquake Engineering Center Technical Report*, 2010.
28. Alireza Farzampour and Matthew R Eatherton. Yielding and lateral torsional buckling limit states for butterfly-shaped shear links. *Engineering Structures*, 180:442–451, 2019.
29. Chang-Hwan Lee, Young K Ju, Jeong-Ki Min, Seung-Hee Lho, and Sang-Dae Kim. Non-uniform steel strip dampers subjected to cyclic loadings. *Engineering Structures*, 99:192–204, 2015.
30. Alireza Farzampour, Iman Mansouri, and Hamzeh Dehghani. Incremental dynamic analysis for estimating seismic performance of multi-story buildings with butterfly-shaped structural dampers. *Buildings*, 9(4):78, 2019.
31. HO Sang, JK Young, and SR Hong. Seismic performance of steel structures with slit dampers. *Eng. Struct*, 31:1997–2008, 2009.
32. K Bayat and B Shekastehband. Seismic performance of beam to column connections with t-shaped slit dampers. *Thin-Walled Structures*, 141:28–46, 2019.
33. Alireza Farzampour and Matthew Roy Eatherton. Parametric computational study on butterfly-shaped hysteretic dampers. *Frontiers of Structural and Civil Engineering*, 13(5):1214–1226, 2019.
34. Alireza Farzampour. *Evaluating shear links for use in seismic structural fuses*. PhD thesis, Virginia Tech, 2019.
35. Jack Moehle and Gregory G Deierlein. A framework methodology for performance-based earthquake engineering. In *13th world conference on earthquake engineering*, volume 679, 2004.
36. Raul D Bertero and Vitelmo V Bertero. Performance-based seismic engineering: the need for a reliable conceptual comprehensive approach. *Earthquake Engineering & Structural Dynamics*, 31(3):627–652, 2002.
37. Ahmed Ghobarah. Performance-based design in earthquake engineering: state of development. *Engineering structures*, 23(8):878–884, 2001.
38. Mohsen Zaker Esteghamati, Jeonghyun Lee, Matthew Musetich, and Madeleine M Flint. INSSEPT: An open-source relational database of seismic performance estimation to aid with early design of buildings. *Earthquake Spectra*, 2020.
39. Mohsen Zaker Esteghamati, Mehdi Banazadeh, and Qindan Huang. The effect of design drift limit on the seismic performance of rc dual high-rise buildings. *The Structural Design of Tall and Special Buildings*, 27(8):e1464, 2018.
40. ICC/SEAOC. *SEAOC Structural/Seismic Design Manual 2009 IBC Vol 4 : Building Design Examples for Steel-Framed Buildings*, 2012.
41. Frank McKenna, Michael H Scott, and Gregory L Fenves. Nonlinear finite-element analysis software architecture using object composition. *Journal of Computing in Civil Engineering*, 24(1):95–107, 2010.
42. American Institute of Steel Construction (AISC), One East Wacker Drive, Suite 700 Chicago, Illinois 60601-1802. *Seismic Provisions for Structural Steel Buildings (AISC 341-10)*, 2010.
43. Dimitrios Vamvatsikos and C Allin Cornell. The incremental dynamic analysis and its application to performance-based earthquake engineering. In *Proceedings of the 12th European conference on earthquake engineering*, volume 40, 2002.
44. Applied Technology Council and United States. Federal Emergency Management Agency. *Quantification of building seismic performance factors*. US Department of Homeland Security, FEMA, 2009.
45. Christine A Goulet, Curt B Haselton, Judith Mitrani-Reiser, James L Beck, Gregory G Deierlein, Keith A Porter, and Jonathan P Stewart. Evaluation of the seismic performance of a code-conforming reinforced-concrete frame building—from seismic hazard to collapse safety and economic losses. *Earthquake Engineering & Structural Dynamics*, 36(13):1973–1997, 2007.
46. Ying Zhou, Pinglan Ge, Mengjie Li, and Jianping Han. An area-based intensity measure for incremental dynamic analysis under two-dimensional ground motion input. *The Structural Design of Tall and Special Buildings*, 26(12):e1374, 2017.
47. Evangelos I Katsanos, Anastasios G Sextos, and George D Manolis. Selection of earthquake ground motion records: A state-of-the-art review from a structural engineering perspective. *Soil Dynamics and Earthquake Engineering*, 30(4):157–169, 2010.
48. Mohsen Zaker Esteghamati and Qindan Huang. An efficient stratified-based ground motion selection forcloud analysis. In *Proceedings of 13th International Conference on Applications of Statistics and Probability in Civil Engineering(ICASP13)*. SNU Open Space, May 2019.

49. Jack W Baker. Efficient analytical fragility function fitting using dynamic structural analysis. *Earthquake Spectra*, 31(1):579–599, 2015.
50. National Institute of Building Sciences, Federal Emergency Management Agency (NIBS, and FEMA). *Multi-Hazard Loss Estimation Methodology Earthquake Model Hazus®-MH 2.1 Technical Manual*, 2012.
51. Brendon A Bradley. The seismic demand hazard and importance of the conditioning intensity measure. *Earthquake Engineering & Structural Dynamics*, 41(11):1417–1437, 2012.
52. Hyun-Ho Lee and Kee-Tae Hwang. Development of the inelastic demand spectra considering hysteretic characteristics and soil condition. 2004.
53. Ricardo A Medina and Helmut Krawinkler. Evaluation of drift demands for the seismic performance assessment of frames. *Journal of Structural Engineering*, 131(7):1003–1013, 2005.
54. Nima Paslar, Alireza Farzampour, and Farzad Hatami. I53nfill plate interconnection effects on the structural behavior of steel plate shear walls. *Thin-Walled Structures*, 149:106621, 2020.
55. Shahram Taghavi and Eduardo Miranda. Estimation of seismic acceleration demands in building components. In *13th World Conference on Earthquake Engineering*, pages 1–6, 2004.
56. Katsuichiro Goda and Solomon Tesfamariam. Multi-variate seismic demand modelling using copulas: Application to non-ductile reinforced concrete frame in victoria, canada. *Structural Safety*, 56:39–51, 2015.
57. Keith A Porter, Anne S Kiremidjian, and Jeremiah S LeGrue. Assembly-based vulnerability of buildings and its use in performance evaluation. *Earthquake spectra*, 17(2):291–312, 2001.
58. Applied Technology Council(ATC). *Seismic Performance Assessment of Buildings Volume 1 – Methodology*, 2018.
59. Mojtaba Dyanati, Qindan Huang, and David Roke. Cost-benefit evaluation of self-centring concentrically braced frames considering uncertainties. *Structure and Infrastructure Engineering*, 13(5):537–553, 2017.
60. CM Ramirez, AB Liel, Judith Mitrani-Reiser, CB Haselton, AD Spear, J Steiner, GG Deierlein, and E Miranda. Expected earthquake damage and repair costs in reinforced concrete frame buildings. *Earthquake Engineering & Structural Dynamics*, 41(11):1455–1475, 2012.
61. Dimitrios Lignos. *Sidesway collapse of deteriorating structural systems under seismic excitations*. PhD thesis, 2008.
62. Seong-Hoon Hwang and Dimitrios G Lignos. Effect of modeling assumptions on the earthquake-induced losses and collapse risk of steel-frame buildings with special concentrically braced frames. *Journal of Structural Engineering*, 143(9):04017116, 2017.